Organometallic Complexes of Graphene: Toward Atomic Spintronics Using a Graphene Web

Stas M. Avdoshenko,[†,*] Ilya N. Ioffe,[‡] Gianaurelio Cuniberti,[†] Lothar Dunsch,[§] and Alexey A. Popov[‡,§,*]

[†]Institute for Materials Science and Max Bergmann Center of Biomaterials, Dresden University of Technology, D-01062 Dresden, Germany, [‡]Chemistry Department, Moscow State University, Leninskie Gory, 119992 Moscow, Russian Federation, and [§]IFW Dresden, Helmholtzstrasse 20, D-01069 Dresden, Germany

ABSTRACT

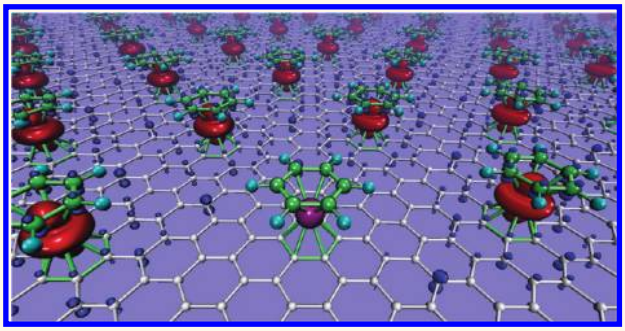

Graphene|metal||ligand systems open a new realm in surface magnetochemistry. We show that by trapping metal atoms in the two-dimensional potential lattice of a graphene−ligand interface it is possible to build a chemical analogue of an optical lattice, a key setup in quantum information and strongly correlated systems. Employing sophisticated first-principles calculations, we studied electronic and dynamic properties of graphene|metal||ligand assemblies and showed that there is a general principle—spin−charge separation in π−d systems—that underlies the possibility of synthesizing and controlling such systems. We find that ligands can work as a local gate to control the properties of trapped metal atoms and can impose bosonic or fermionic character on such atomic nets, depending on the ligand's nature. Remarkably, the magnetization energy in such systems reaches record-high values of *ca.* 400 meV, which makes the respective magnetic phenomena utilizable at room temperature. Accompanied by spin polarization of the graphene π-conjugated system it leads to spin-valve materials and brings the realization of quantum computing one step closer.

KEYWORDS: graphene · spin valve · organometallic chemistry · sandwich complex · spin−charge separation · quantum computing

Graphene[1,2] and graphene-like structures (ribbons, flakes, *etc.*) attract rapidly growing interest in the scientific community due to their amazing properties. One of the hottest topics in this field is graphene magnetism and its potential spintronic and quantum information applications.[3,5] Much hope was vested in the preservation and transport of spin information in 1D and 2D systems in pure,[5] defected,[5−7] or functionalized graphene structures.[8,9] These phenomena are widely discussed in the context of structural defects or a special chemical functionalization of graphene, but practical implementations are still under theoretical and experimental consideration. The most crucial obstacle is that even if a weak magnetism in the graphene-based systems is possible, the theoretically predicted (anti/ferro)magnetic transition temperature is too low for practical applications.[10]

The ultimate goal in the field of quantum computing and spintronics is to achieve an architecture in which one bit is represented by the simplest possible unit, a single atom.[11,12] Implementation of such hypothetical[13] or complicated[14,15] devices requires the solution of several important problems. First, they must be simple in their design and stable under the conditions of use. Second, there must be an easy way to access and control qubit network states.

In many respects, endohedral fullerenes became promising candidates for molecular spintronics[16,17] since their stable carbon cages isolate encapsulated magnetic species from aggressive environments.[18,19] However, establishing a reliable communication/access net within a qubits array based on endohedral fullerenes is extremely complicated.[17,19] A proposed solution based on single-wall carbon nanotubes is also not straightforward.[19] A creative realization of the quantum computing network in optical lattices with ultracold atoms trapped in an external potential proved very stable and controllable but apparently very expensive and poorly suited for mass production.[13,17] Likewise, the design of quantum entangled system at room temperature via liquid-state nuclear magnetic resonance technique is also a fascinating but still rather complicated alternative.[22] Here we report a conceptually new and chemically accessible way to

* Address correspondence to savdoshenko@nano.tu-dresden.de; a.popov@ifw-dresden.de.

Received for review September 28, 2011 and accepted October 31, 2011.

Published online October 31, 2011
10.1021/nn203719a

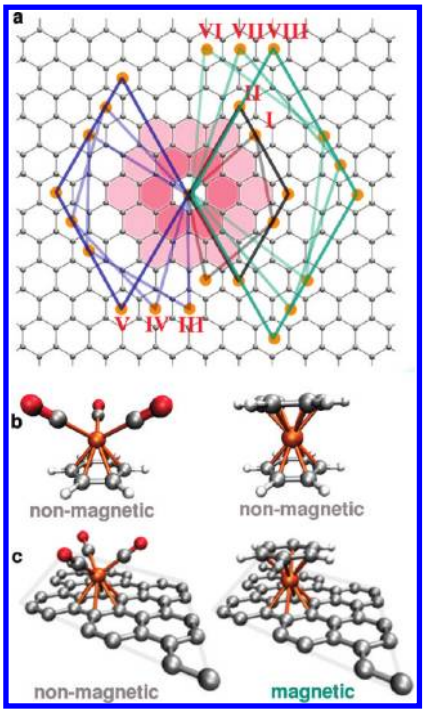

Figure 1. (a) Unit cell topology of the graphene|Cr|ligand (G|Cr|L) systems analyzed in the present report. The surface distribution of the Cr|L elements determines the substrate symmetry and, consequently, its electronic properties. (b) Typical π-ligand molecular complexes of Cr. (c) Optimized structures of different G|Cr|L systems.

construct a net of spin states on a graphene substrate by assembling sandwich-like graphene|metal||ligand (G|Me|L hereafter) structures as shown in Figure 1. An archetypical complex, bis(benzene)chromium, $Cr(C_6H_6)_2$, and a broad variety of its well-known analogues and derivatives can serve as molecular prototypes of such systems (Figure 1).[20] Formation of stable periodical G|Cr|L systems with different unit cell size and ligand types is predicted, and the spin polarization strength is found to be a function of the structure topology and ligand's nature. We show that by sequential replacement of substituents in the π-ligand arene it is possible to fine-tune the properties of the G|M|L system within a remarkably broad range: from ferromagnets with high magnetization energy of up to 400 meV, through exotic and unexpectedly stable systems with an almost flat band at the Fermi level, to open-gap graphene materials sought after in industrial applications. These electronic phenomena are discussed in connection with the spin−charge separation,[23,24] a fundamental principle revealed for the systems with π−d interactions. Finally, high thermal stability of G|M|L systems is proved by means of *ab initio* molecular dynamics.

RESULTS AND DISCUSSION

Studied Systems. High mobility of heteroadatoms on the surface of crystalline substrates and their affinity to surface defects preclude construction of single-atomic quantum dot arrays in a regular controllable manner. Furthermore, due to unsaturated valence and induced spin, an isolated atom can be very reactive. In this regard, it is unlikely that the widely studied hybrid graphene/metal systems[25−35] with single metal atoms regularly distributed over the graphene sheets can be obtained experimentally on a large scale or as a working element.[9] At the same time, organometallic chemistry provides multiple examples of stable systems, where d- or f-metal atoms are "trapped" within the framework of suitable ligands.[20] In the case of arene π-ligands, the metal atoms can retain their formal zero oxidaton state (although the ligand field splits the frontier d-orbitals), while the π-system of the ligands remains relatively unperturbed. Yet, such complexes often exhibit enhanced stability; for instance, the dissociation temperature of $Cr(C_6H_6)_2$ and (benzene)-chromium tricarbonyl, $Cr(C_6H_6)(CO)_3$, is about 600 K.[36] Hence, considering the graphene sheet as an extended π-system with multiple addition sites, synthesis of stable G|Cr|L complexes retaining unique electronic properties of graphene is much more feasible than the synthesis of graphene complexes with bare metal atoms. The synthetic routes to sandwich and half-sandwich complexes of transition metals (such as the aforementioned $Cr(C_6H_6)_2$ and $Cr(C_6H_6)(CO)_3$) are well established in the field of organometallic chemistry.[20] For instance, $Cr(CO)_6$ readily reacts with arenes, forming Cr(*arene*)$(CO)_3$ complexes, and utilization of the same synthetic strategy for graphene is straightforward. The synthetic route toward G|Cr|(ligand) systems might include the methods of wet chemistry developed for the synthesis of sandwich and half-sandwich compounds[20] or CVD-like techniques.[21] Further exploration of the possible synthetic routes to G|Cr|L complexes is beyond the scope of this work; here we only emphasize that appropriate methodologies are within the core knowledge of organometallic chemistry. We will show below that, once created, G|Cr|L systems such as shown in Figure 1c provide unique possibilities for combining electronic properties of graphene with those of transition metals.

As a basic initial test case, we consider a family of G|Cr|(C_6H_6) systems, in which $Cr(C_6H_6)$ moieties are periodically distributed over the graphene sheet, preserving its hexagonal symmetry. To study remote through-graphene interaction of the Cr centers, eight systems (labeled I−VIII as shown in Figure 1a) with gradually increasing inter-Cr distance and corresponding unit cell size were studied: the smallest cell allowed by the ligand-imposed steric limitations has an edge length of 6.55 Å (system I), while the largest considered cell size reaches 12.34 Å in system VIII. According to the structure of their first Brillouin zone, these eight systems can be classified into two families with different 2D-k-dispersion topology (*i.e.*, the Γ-M-K-Γ band structure). For those systems, whose unit cell does

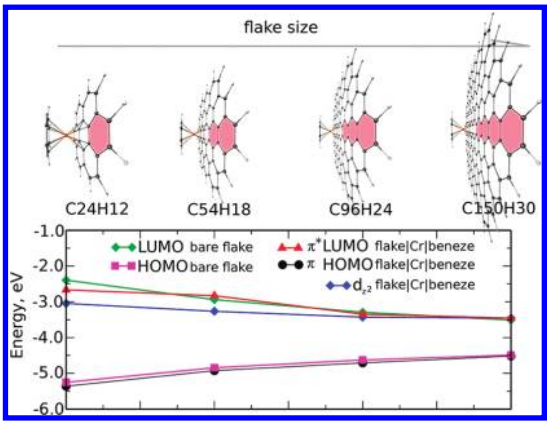

Figure 2. Frontier MO energies of finite systems flake|Cr|-(C_6H_6) as a function of the flake size. For the $C_{96}H_{24}$|Cr|(C_6H_6) complex, the d_{z^2}-derived MO is almost degenerate with the π^*-states of the flake, and geometrical characteristics of the complex are similar to those of the systems VI–VII.

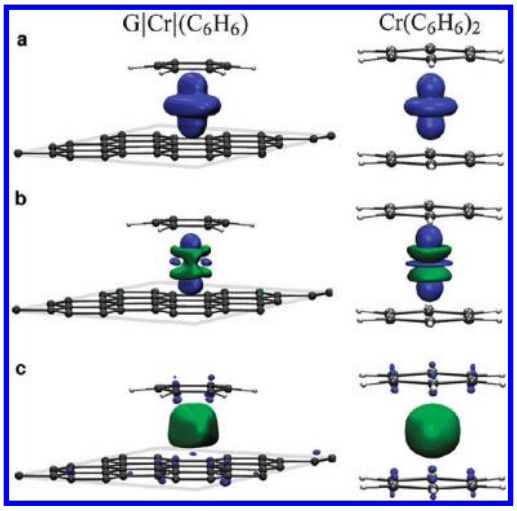

Figure 3. Real-space representation of spin–charge separation in the molecular system $Cr(C_6H_6)_2$ (right row) and G|Cr|(C_6H_6) (left row): (a) spin density, $\Delta_{spin}^{\alpha/\beta}(r)$, in G|Cr|($C_6H_6$) and a cation of $Cr(C_6H_6)_2$; (b) difference of the electron density induced by the removal of an electron, $\Delta_{el}^{0/+1}(r)$ (for the G|Cr|L system it is a difference of the densities of the spin-polarized and nonpolarized solutions); (c) spatial distribution of the spin–charge separation hole for $Cr(C_6H_6)_2$ and G|Cr|(C_6H_6).

not include 6*n* carbon atoms (systems I, IV, V, VI, and VIII), the band extremes around the K-point are reminiscent of graphene. In the remaining cases (the number of atoms in the unit cell is equal to 6*n*, as in G|Me|L systems II, III, and VII) the critical points of the bands are shifted to the Γ-point, and these systems tend to have a more open gap.[37] Importantly, such systems are all-benzenoid in terms of Clar's theory. This dichotomy closely resembles the difference in the band structure between *zig*zag and armchair graphene ribbons.[6,37] Certainly, for the nonderivatized graphene sheet this classification is only formal, but when the symmetry of the G|Cr|L system is determined by the position of Cr|L moieties, the electronic structure of the above two families is definitely different.

Electronic Structure of $Cr(C_6H_6)_2$ and Spin–Charge Separation. Before proceeding to the studies of extended G|Cr|L systems, we briefly review the electronic structure of $Cr(C_6H_6)_2$ and illustrate the phenomenon of the spin–charge separation accompanying the electron transfer in this and all other π–d systems. The electronic structure of $Cr(C_6H_6)_2$ has been studied since the 1950s.[38,40] Two parallel benzene rings in an eclipsed conformation form a D_{6h} symmetric pattern in which a degenerate set of 3d atomic orbitals of Cr is split into e_{1g}^4, a_{1g}^2, and e_{2g}^0 molecular orbitals (MOs; the superscript denotes their occupations). The e_{1g} MO originates from d_{xz} and d_{yz} AOs of Cr considerably mixed with benzene MOs to form Cr–benzene bonding MOs of a hybrid nature. On the contrary, the a_{1g}-HOMO is essentially the pure d_{z^2} AO of the Cr atom. The gap between the Cr-localized HOMO and the ligand-localized LUMO can be modified by changing the arene system. Substituting one of the benzene ligands in $Cr(C_6H_6)_2$ with coronene, $C_{24}H_{12}$, circumcoronene, $C_{54}H_{18}$, or larger graphene flakes $C_{96}H_{24}$ and $C_{150}H_{30}$, we observed that the gap drops almost to zero (Figure 2), pointing to the possibility of crossing of the graphene and Cr-based bands in extended systems. Electron redistribution accompanying such crossing, which is indeed found in G|Cr|L systems as discussed below, can be understood by applying the concept of spatial spin–charge separation illustrated in Figure 3 and explained in the following paragraphs.

HOMO localization on the Cr atom in $Cr(C_6H_6)_2$ naturally implies that one-electron oxidation should result in a radical-cation with spin density closely resembling the orbital density of the d_{z^2} AO of Cr. This obvious expectation is, indeed, confirmed both experimentally[41] and computationally (Figure 3a). Likewise, removal of one electron from the d_{z^2} orbital of Cr implies that the atomic charge of Cr, *q*(Cr), could also be changed by approximately one charge unit. However, we found, quite counterintuitively, that the charge on Cr in $Cr(C_6H_6)_2^+$ is virtually identical to that in the neutral $Cr(C_6H_6)_2$. Keeping in mind the ambiguity in the definition of the atomic charge, we tested different schemes to compute atomic populations (Bader, Mulliken, NBO), and all of them demonstrated only negligible change of the *q*(Cr) value upon electron detachment. Thus, there is an apparent paradox dubbed as "spatial spin–charge separation": while the net electron density is withdrawn from the benzene ligands, the spin density is localized on the metal atom. It is convenient to illustrate the manifestation of the spin–charge separation through the analysis of the differential electron density comparing the neutral and charged states, $\Delta_{el}^{0/+1}$, shown in Figure 3b. Instead of the single positive density lobe anchored to the metal atom similar in its shape to the $\Delta_{spin}^{\alpha/\beta}$, a more complex pattern is found for the $\Delta_{el}^{0/+1}$. The domains of alternating sign found for $\Delta_{el}^{0/+1}$ in the

TABLE 1. Relative Energies of Ferromagnetic (spin-polarized) Phase Solutions for Structures I–VIII with Respect to Nonmagnetic (spin-unpolarized) Ones (EM), Magnetic Exchange Energy (*J*),[a] the Total Magnetic Moment of Each System (μ), and the Distance between Localized Magnetic Centers (*d*(Cr–Cr))

	I	II	III	IV	V	VI	VII	VIII
EM, meV	335.0	−107.0	−404.0	−25.0	−41.0	−173.54	−156.0	−140.0
$J(2 \times 2)$, meV	−10.0	−80.0	−324.0	−17.0	−31.0	−123.5	−136.0	−130.0
μ, μ_B	0.19	0.14	0.22	0.37	0.30	0.34	0.23	0.30
d(Cr–Cr), Å	6.541	7.452	8.599	8.919	9.877	10.749	11.331	12.338

[a] *J* is defined as the energy difference between fully ferromagnetic state (↑↑↑↑) and the state with the flipped spin for one Cr atom (↑↑↑↓) computed for the 2×2 supercell.

vicinity of the metal atom cancel each other, so that the integral change of the *q*(Cr) value is negligible.

Thus, for the purposes of analysis of the electronic structure it may be convenient to formally decompose one-electron oxidation of $Cr(C_6H_6)_2$ into two steps (of course, inseparable in reality): (i) removal of one electron from the d-orbital of Cr followed by (ii) adjustment of the electronic density of the whole system. The spatial distribution of the spin density is a real space presentation of the first formal step. Importantly, the spin density obtained at this step remains mostly unchanged after the second step. The second step, in turn, can be best illustrated using the concept of spin–charge separation hole (SCSH), defined as $\Delta_{SCSH} = \Delta_{el}^{0/+1} - \Delta_{spin}^{\alpha/\beta}$. An isodensity plot of Δ_{SCSH} (Figure 3c) clearly shows how the electron density is shifted from the ligands toward the Cr atom: an almost spherical domain of the density concentration is formed around the Cr atom, while benzene fragments accommodate smoothly the delocalized domain of the density depletion.

Importantly, such behavior is not a unique feature of the $Cr(C_6H_6)_2$ complex but rather represents a common property of any metal–ligand system. For instance, Figure S1 (see Supporting Information) shows analogous graphs for $Cr(C_6H_6)(CO)_3$. A similar picture was also observed in endohedral metallofullerenes and in other transition metal complexes with π-ligands.[24,42] To ensure that the spin–charge separation is not an artifact of a single-determinant approach or of the DFT approximation, we verified the shape of the $\Delta^{0/+1}$ function at the MCSCF/cc-pVTZ level of theory with single to quadruple excitations within the active space covering the π-orbitals of benzene ligands as well as 3s–3d and 4s–4d orbitals of Cr and found it virtually indistinguishable from the DFT-computed function depicted in Figure 3b. It also must be noted that the spin–charge separation is strongly related to the phenomenon of charge preservation in transition metals discussed earlier by Raebiger *et al.*[23]

Quantum Web. Generalization of the electronic structure of $Cr(C_6H_6)_2$ to extended systems is straightforward. As was noted above, an increase in size of one of the arene ligands leads to gap shrinking in the limit of an infinite 2D system such as G|Cr|(C_6H_6) (Figure 2). For all G|Cr|(C_6H_6) systems considered in this work with topologies ranging from I to VIII (Figure 1), the spin-unpolarized solutions at the PBE level give an almost dispersionless d_{z^2}(Cr)-based band, which is pinned from below to the conduction bands of the graphene subsystem. Importantly, these localized states define Fermi levels of the G|Cr|(C_6H_6) systems as a whole, which results in a very unusual electronic situation for infinite systems: a flat band at the Fermi level. It is well known from the condensed matter theory that a flat band at the Fermi level is an indication of system instability. On the other hand, it is also a marker of the broad range of specific phenomena from magnetism to superconductivity or superfluidity.

However, it is the spin-polarized (*i.e.*, magnetic) solution that is predicted to be the ground state in G|Cr|(C_6H_6) systems II–VIII. Using the commonly accepted definition of the energy of magnetization (EM) for periodic systems as the difference between the energy of the spin-polarized and spin-unpolarized solutions, we found that the EM values for G|Cr|(C_6H_6) systems can reach up to 400 meV per magnetic center (Table 1), a record-high value among the systems of such kind. The EM noticeably depends on the topology (in particular, on the distance between metal centers; this point will be discussed in detail below). At the same time, the total magnetic moment for all topologies remains in the range 0.2–0.3 μ_B. To ensure that the ferromagnetic state is indeed a ground state for the majority of structures considered, we performed additional computations with 2×2 supercells flipping the spin on one of the Cr centers. Except for system I, the energy difference between fully ferromagnetic and spin-flipped states was always negative and agreed well with the EM values listed in Table 1. The reason for high stability of the ferromagnetic phase is discussed below.

As noted above, G|Cr|(C_6H_6) structures are classified into two families depending on their topological relations to the bare graphene. These two families yield different k-dispersion patterns, as illustrated by the band structures of systems VI and VII plotted in Figure 4a,d. The spin-polarization manifests itself in the splitting of still essentially flat $Cr(d_{z^2})$-derived bands. The effect of the spin polarization on the other bands is almost negligible and can be observed only in the close proximity of the Fermi level. Spin-polarized density-

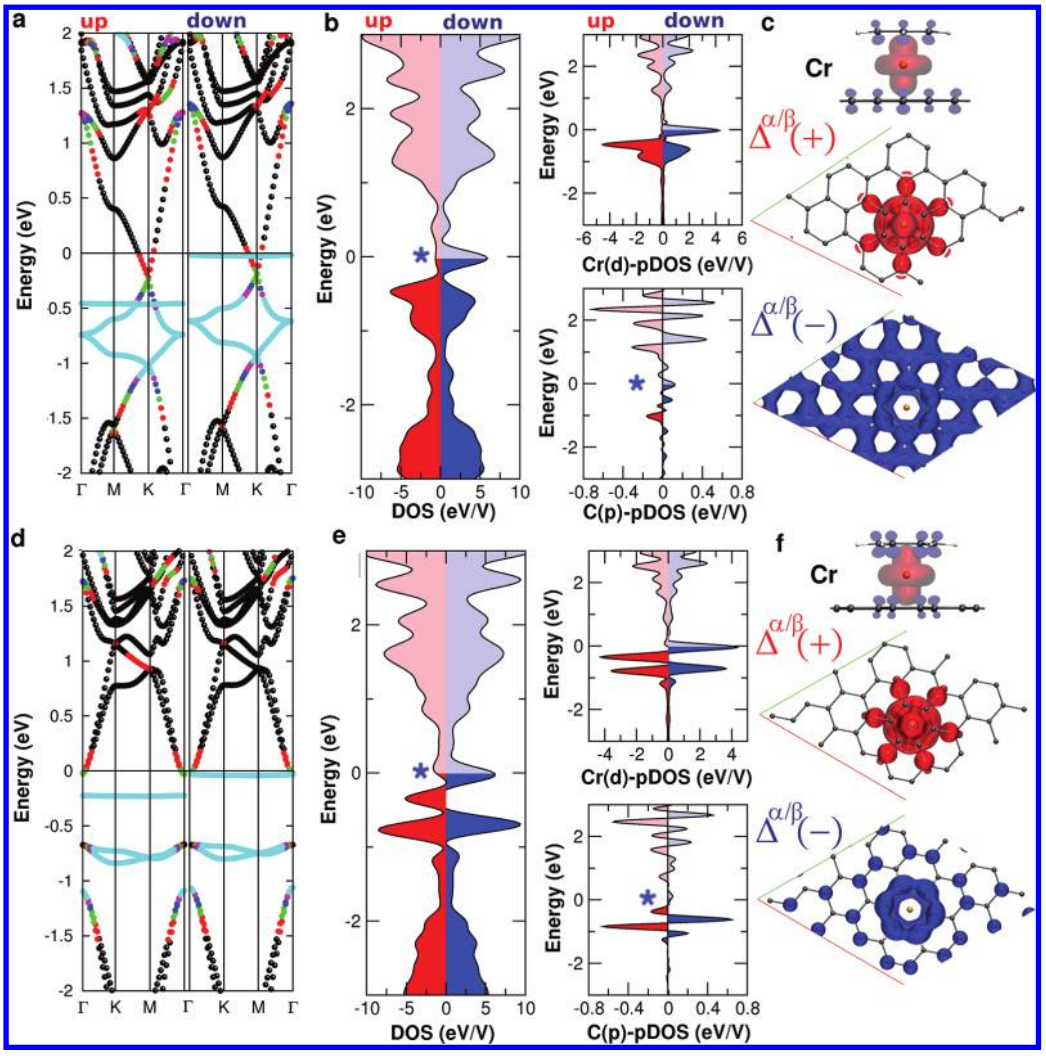

Figure 4. Electronic structure for the representative G|Cr|(C_6H_6) systems VI and VII. (a and d) Spin-polarized solution of band structure profiles (color scheme: d_{Cr} contribution in 10−20% (red), 20−30% (green), 30−40% (blue), 40−50% (magenta), >50% (cyan)). (b and d) Spin-dependent full DOS profiles evidence spatial splitting of up- and down-spin states. In particular, spin-down states are localized at Cr centers, whereas the complementary spins are imprinted in the graphene π-states. This fact can also be seen in the real space spin density distribution (c and f), where excess spin-up density is homogeneously distributed over the graphene substrate.

of-states (DOS) for both families exhibits a sharp feature at the Fermi level, which assigns the G|Cr|(C_6H_6) systems to ferromagnetic materials according to the Stoner criterion. Projection of the DOS of the metal and graphene subsystems (Figure 4b,e) shows that the magnetism of G|Cr|(C_6H_6) is mostly determined by spatial and energetic localization of the excess (up) spin on the metal centers (presumably in Cr-d_{z^2}-derived states). The spin polarization of the graphene substrate remains negligible; however, the spin-down states of graphene appear around the Fermi level. The magnetic moment of the graphene subsystem thus amounts to *ca.* 0.1 μ_B and is antiparallel to the local magnetic moments of the metal centers. This pattern is common for all G|Cr|(C_6H_6) systems studied in this work and has pronounced similarities to the results of some recent experimental and theoretical studies of the magnetic properties of graphene−metal interfaces.[39,43]

Similar oscillation behavior of the magnetic coupling in dependence on the intermetallic distances was described earlier on the surface of carbon nanotubes[44] and explained in terms of the RKKY model.[45] However in this particular case, a contribution of Kondo coupling[46] interaction has to be specifically studied and will be reported elsewhere.

The origin of the spin-polarized states imprinted in the graphene substrate and for the accompanying redistribution of the electron density can be discussed in terms of the spin−charge separation hole introduced in the previous section. It also shows some similarity to the recently described image potential states in graphene.[43] In the molecular system Cr(C_6H_6)$_2$, the SCS is induced by removal of one electron; in G|Cr|-(C_6H_6) an analogous effect is caused by crossing of the Cr-d_{z^2}-derived localized band and conduction band of the graphene substrate. This crossing results in a partial

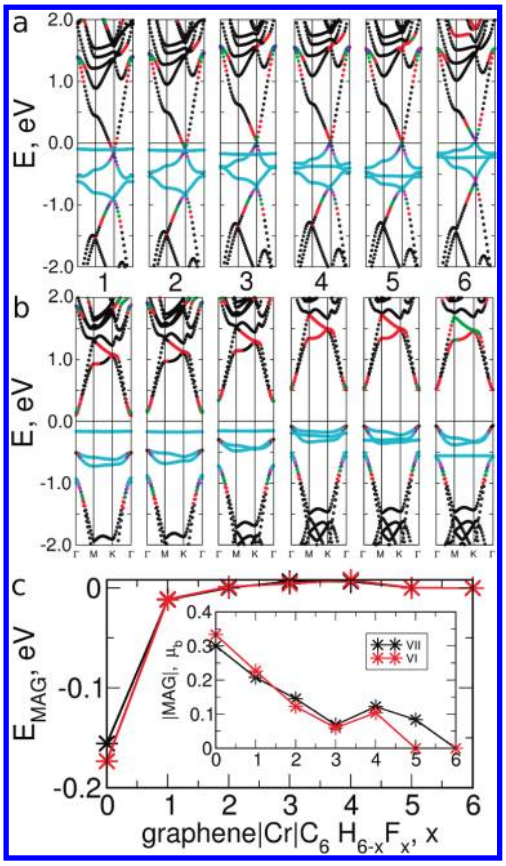

Figure 5. Evolution of the electronic structure of the G|Cr|-$C_6H_{6-x}F_x$ system (topologies VI and VII) with the gradual substitution of hydrogen with fluorine atoms in the benzene ring (x = 1−6). (a, b) Response of the spin-up band structure to the fluorine substitution (negative "local gate") for the systems VI (a) and VII (b) (color scheme: as in Figure 4). (c) Full magnetic moments (inset) and magnetization energies ($E^{FM}_{total} - E^{NM}_{total}$) of the G|Cr|$C_6H_{6-x}F_x$ as a function of x.

spin-polarized transfer of the electron density from the Cr-d_{z^2} states to graphene. However, the metal-to-graphene electron transfer is balanced by formation of the SCSH (Figure 3c). Readjustment of the charge density within the graphene and the π-ligand groups enforced by the SCSH results in the imprinted charge density in the carbon network, which is complementary to the induced spin on the metal centers. As can be clearly seen from the spin-resolved projected DOS and band structures, both systems VI and VII have half-metallic nature. Independent of the topology, spin-up states of the metal have an excess at the Fermi level, but these states are strongly localized and of low carrier mobility (velocity at the Fermi level is about zero). However, less pronounced contribution of graphene spin-down states at the Fermi level can still enable formation of a conductive π-conjugated net over the graphene substrate, as can be seen in Figure 4c,f. Formation of such a net is a necessary prerequisite for the material to be classified as a spin-valve with a possibility to address and manipulate localized and seemingly disjointed but yet coupled atomic networks.

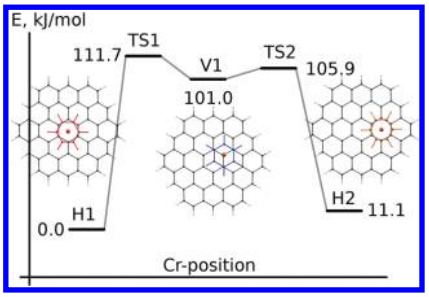

Figure 6. Energy profile for the migration of the Cr|(C_6H_6) moiety on the surface of the graphene flake.

TABLE 2. Relative Energies of the PES Critical Points (kJ/mol) Computed at the Different Level of Theory with PBE/TZ2P-Optimized Coordinates (def2 stands for the def2-TZVP basis set)

CP	PBE/TZ2P	PBE/def2	PBE-D/def2	PBE0/def2	B2PLYP/def2	B2PLYP-D/def2	M06/def2
H1	0.0	0.0	0.0	0.0	0.0	0.0	0.0
TS1	111.7	118.4	128.9	151.3	140.1	147.9	141.4
V1	101.0	107.5	118.4	139.8	122.9	130.9	119.2
TS2	105.9	112.3	122.5	146.8	130.4	137.8	131.3
H2	11.1	11.7	13.5	20.5	20.5	21.8	20.1

Variation of the EM values between different G|Cr|-(C_6H_6) topologies can be thus correlated to the way in which π-system of the pristine graphene substrate can account for additional charge density. The spin-polarized solutions are stable when spin-down states can form conjugated π-systems similar to those shown in Figure 3c,f for systems VI and VII. However, as the surface density of the metal centers increases (which is also reflected in a more pronounced dispersion of the Cr-d_{z^2} band), a repulsive Coulomb interaction overcomes the energy gain from the formation of the conjugated π-system and destabilizes the ferromagnetic state, as found for system I, with the shortest Cr−Cr distance.

Arene Ligand As a Local Gate. So far we have shown that the electronic properties of G|Cr|(C_6H_6) systems are determined by the interplay between the dispersionless band derived from the local Cr-d_{z^2} states and the conduction band of the graphene substrate. The contribution of the benzene states to the total DOS in the range of $E_F \pm 2$ eV is negligible, and hence the role of the π-ligand is seemingly unimportant. In fact, this impression is deceptive, because the structuring of the d-orbital pattern of chromium and preservation of the graphene band structure in G|Cr|(C_6H_6) is only possible in the presence of the benzene rings coordinating the metal atoms (compare to the bare Cr atom on the graphene surface described by Valencia *et al.*).[29] Furthermore, it is obvious from the electronic structure shown in Figure 4 that the properties of the G|Cr|*arene* assemblies can be fine-tuned by modulating the

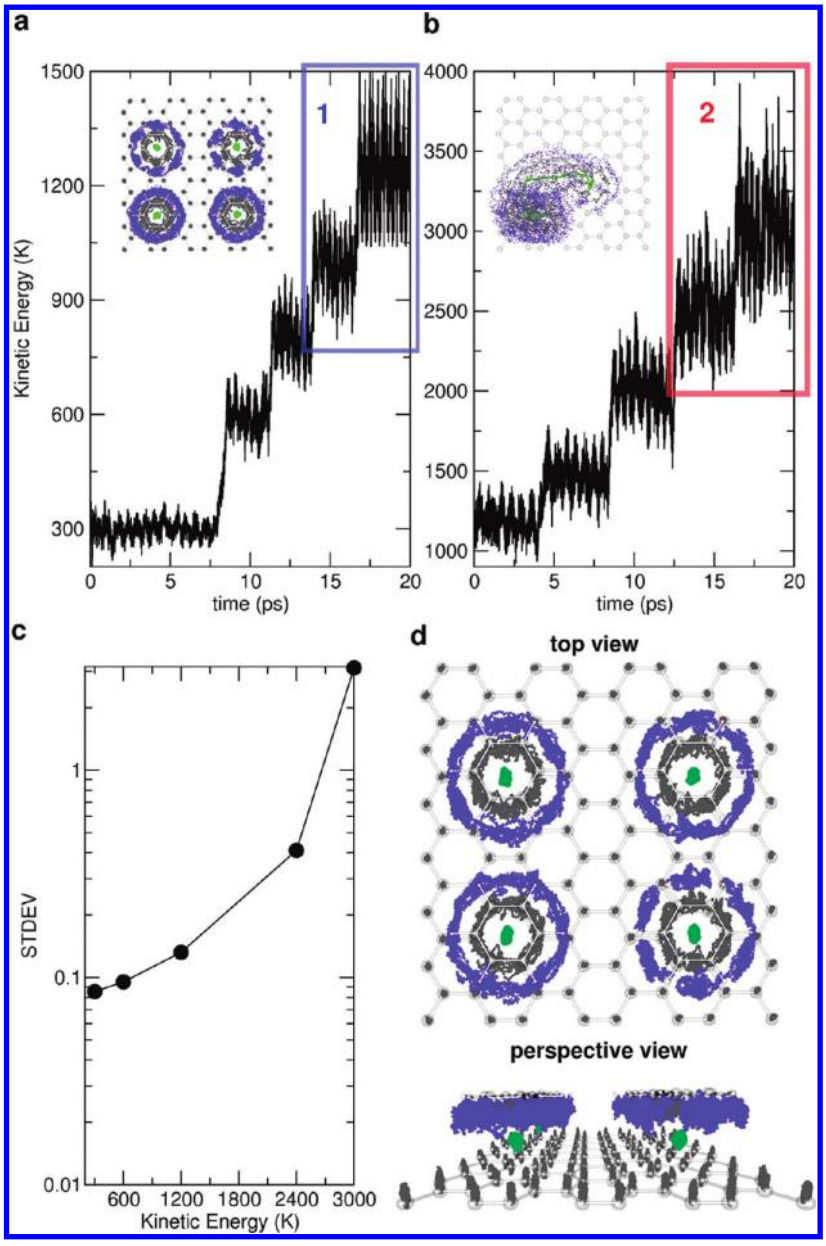

Figure 7. Time profile of the kinetic energy for the Γ-point Nosé-Hoover dynamics of the supercell G|{Cr|(C_6H_6)}$_y$ with $y = 1$ (a) and 4 (b) at different temperatures in the range 300−3000 K and 2 ps time window at each thermostat temperature. (c) Standard deviation (STDEV in Å) logarithmic plot shows that even at a relatively high NVT-bath temperature of 1200 K, the Cr position is well-localized. (d) Top and perspective views of room-temperature behavior in the system: Cr atoms are localized above the centers of hexagonal rings of graphene, while benzene rings rotate freely.

position of the Cr-d_{z^2} level with respect to the graphene bands. We have found that the π-ligands provide an ideal highly flexible framework for this purpose. Introduction of electron-donating or electron-withdrawing substituents in the benzene ring has a dramatic impact on the energy of the Cr-d_{z^2} level, leaving the other bands almost intact. Figure 5 illustrates the action of the gradual hydrogen-to-fluorine substitution in benzene rings of G|Cr|(C_6H_6) systems VI and VII.

At the initial stages of substitution ($x < 3$) the Cr-d_{z^2} band and the Fermi level are shifted to lower energy with respect to graphene and Gr-$d_{xz,yz}$ bands. This results in a drastic drop of the ME values and magnetic moments and, ultimately, in the preference of the spin-unpolarized solution for medium and large degrees of substitution. For $x > 4$ (VI) or 3 (VII) the E_f and graphene bands remain fixed, while the Cr-d_{z^2} level is shifted further down below one of the Gr-$d_{xz,yz}$ band(s). The respective consequences are different depending on the substrate topology. For system VII, these transformations open the gap and produce a spin-unpolarized system with the flat band near the Fermi level for $x =$ 2−3 and a semiconductor with pronounced p-type character for larger x (Cr-d_{z^2} level is below the Cr-$d_{xz,yz}$ band). For the topological pattern VI the situation is even more spectacular. The gap remains closed for any

x, and the unpolarized solutions are more preferable by *ca.* 25 meV. One thus obtains a zero-gap material with linear dispersion at the Fermi level. Remarkably, in this system the Dirac cones[2,47] are not formed by the crossing of pure carbon π-bands as in the pristine graphene, but rather originate from the intersection of the π-carbon and d-metal bands. Whereas velocity of the massless particles at the Fermi level (v_F) in graphene is precisely 0.003*c*, v_F deviates in the range 0.001−0.003*c* for the π-carbon/d-metal band crossing. Large contributions of the metal d-states in the conductive bands also recall a d-pairing state in some high-temperature superconducting materials.[48] A band structure similar to that of G|Cr|($C_6H_3F_3$) systems VI and VII is also found for isostructural assemblies G|Cr|-$(CO)_3$, in line with the electron-accepting action of three CO ligands (see SI). Thus, the arene ligand serves as a local gate that can be used to fine-tune the properties of the G|Cr|*arene* architecture without modifying the graphene substrate or changing the metal atom.

Stability of G|Cr|(C_6H_6). I. Energy Profile. Successful application of the unique electronic properties of G|Cr|-*arene* architectures strongly depends on their stability. Mobility of the Cr|*arene* units on the graphene substrate or even their detachment may impose severe limitations to the practical realization of such architectures. To address this issue, we have studied the possibility of the Cr(C_6H_6) migration (obviously, detachment barriers should be higher than those of the surface migration). To study stability of the G|Cr|(C_6H_6) toward migration of Cr|(C_6H_6) units over the graphene surface, we have performed two types of calculations. In a "static" approach, a fragment of a potential energy surface (PES) for the ($C_{54}H_{18}$)|Cr|(C_6H_6) complex was analyzed by means of the intrinsic reaction coordinate (IRC) approach. In particular, we have looked for the path and the barrier to the migration of the Cr|(C_6H_6) unit from the central ring (H1, ΔE = 0.0 kJ/mol) to the neighboring ring (H2, ΔE = 11.1 kJ/mol; see Figure 6 for the structures and schematic description of the reaction coordinate). PBE/TZ2P calculations have shown that migration occurs through an intermediate vertex state (V1) in which Cr is located above the carbon atom. This state (ΔE = 101.0 kJ/mol) forms a shallow minimum between two transition states (TS1 and TS2, ΔE = 111.7 and 105.9 kJ/mol, respectively) with similar structures (in each TS, Cr is slightly displaced from the vertex position toward the center of the corresponding ring). Thus, at the PBE/TZ2P level the barrier to migration exceeds 100 kJ/mol.

For all five critical points, we have also performed point energy computations using different density functionals and the def2-TZVP basis set.[62] The functionals used were PBE(-D), PBE0, B2PLYP(-D), and M06; here D stands for the empirical Grimme's correction for van der Waals interactions,[57−61] B2PLYP is a double hybrid functional combining DFT- and MP2-derived correlation energy,[59,60] while M06 is a hybrid functional from the Minnesota family that was shown to give especially good results for transition metal complexes and reaction barriers.[63] As can be seen in Table 2, the use of hybrid DFT functionals and Grimme's dispersion correction increased the relative energies of the transition states, thus predicting the H1 and H2 states to be even more kinetically stable than at the PBE level.

Stability of G|Cr|(C_6H_6). II. Molecular Dynamics. Dynamic stability of the G|Cr|(C_6H_6) system was also probed by means of DFT-based Both−Oppenheimer molecular dynamics. Two testing systems with dense and sparse distributions of Cr|(C_6H_6) moieties as shown in Figure 7 were first equilibrated for 10 ps at 300 K, and then the temperature was increased in several steps up to 3000 K with the analysis of the system evolution for several picoseconds at each temperature step. Computations were performed in the Γ-point with a Nosé-Hoover thermostat.

This study revealed that both studied systems exhibit unusual stability up to 2000 K. Even at the highest studied temperatures, when graphene itself already exhibited giant out-of-plane vibrational deformations, Cr|(C_6H_6) remains tightly bound to the surface, showing only rotational motions around the Cr−graphene axis. For a system with dense packing, this dynamic behavior was sustained during further heating; however for a less dense packing of Cr|(C_6H_6) units migration of the metal center started above 2000 K (Figure 7), but detachment was not observed up to the limit of 3000 K.

CONCLUSIONS

In this work we introduce a chemical route to the network of well-separated qubits represented by single metal atoms with arene ligands trapped in a periodic potential well of a graphene layer, (G|Me|L), which opens a way to quantum routing and state manipulation through the conductive graphene substrate. In particular, we describe two regular families of these networks, with and without graphene-like band structure. In both families of G|Cr|(C_6H_6) systems we found ferromagnetic ordering in the ground electronic state with high magnetization energy (up to 400 meV). The Cr|*arene* quasi-atoms carrying spin information are spatially isolated from each other in the periodic potential created by the graphene substrate. Nevertheless, they still interact with each other *via* a spin communication net within the graphene layer. We explained these phenomena on the basis of spin−charge separation, a fundamental property of the systems with π−d interactions. Moreover, we propose an efficient and experimentally feasible[49] approach to control the electronic properties of these systems by using the arene ligand as a local gate. Thus, by varying the number of substituents in the

G|Cr|($C_6H_{6-x}F_x$) system it was possible to achieve either an open-gap state or a zero-gap material with linear dispersion at the Fermi level provided by the interplay of π^* graphene and localized 3d metallic states. The high thermal stability of such architectures, proved by *ab initio* molecular dynamics simulations, provides a solid background for their practical realizations.

COMPUTATIONAL DETAILS

The use of several molecular and periodic codes for computations was dictated by the large size of the studied systems, and hence the most efficient approach was used for each type of computations. Data were visualized with the VMD[50] package.

Geometry and 2D Electronic Properties. VASP[51] was employed as a periodic wave function code. For these calculations, the projector augmented wave method within general gradient approximation proposed by Perdew, Burke, and Ernzerhof (PBE)[52] for the exchange and correlation functional part was chosen. The Kohn–Sham orbitals were expanded as a set of plane-wave bases up to 550 eV. The Brillouin zone is sampled with a $4 \times 4 \times 1$ Monkhorst–Pack k-point grid. The Vanderbilt's ultrasoft pseudopotentials[53] with plane-wave energy cutoff were chosen to be 58 Ryd. The $11 \times 11 \times 1$ Monkhorst–Pack grid was used for the calculation of the density of states for all structures I–VIII. The geometry optimization of the internal coordinates with fixed cell parameters (corresponding to the bare graphene) proceeded until Hellmann–Feynman forces were less than 0.01 eV/Å. The relative energies for different magnetic configurations were converged within 1 meV according to the energy cutoff and limit of the k-point grid.

Intrinsic Reaction Coordinate and Single-Point Calculations. The energy profile of the Cr|(C_6H_6) migration pathway in the ($C_{54}H_{18}$)|Cr|(C_6H_6) complex was computed using PRIRODA[54] at the DFT|PBE|TZ2P level. Single-point calculations were then performed using ORCA code[56] at the DFT|X|def2-TZVP level, where X stands for PBE(D), PBE0, and B2PLYP(D),[57–61] and by using the Gaussian09[64] code at the DFT|M06|def2-TZVP level. Computations at the MCSCF/cc-pVTZ level of theory were performed using the Firefly package.[65,66]

Molecular Dynamics. Born–Oppenheimer Γ-point molecular dynamics with the Gaussian and plane wave GPW scheme[67–70] were performed with the PBE exchange–correlation functional[52] in CP2K code. The electron–ion interaction was described by the Goedecker–Teter–Hutter pseudopotentials[67–69] and the TZV2P/DZV2P basis. Canonical (NVT) ensemble with a 300 K bath temperature and Nosé-Hoover chains with a 200 fs coupling rate was used for initial equilibration (10 ps). The stability of the system was then studied by means of heating steps in the 300–3000 K temperature range with 600 K steps. Minor deviations between the Pade-LDA and PBE results found during the initial equilibration at 300 K enabled the use of the Pade-LDA method for all further studies.

Acknowledgment. S.M.A. is thankful for financial support from the Erasmus Mundus Programme External Co-operation (EM ECW-L04 TUD 08-11). Financial support from DFG (grant PO 1602/1-1 to A.A.P.) and RFBR (grant 09-03-00353 to I.N.I.) is gratefully acknowledged. The authors thank TU Dresden for computing time on high performance computers at ZIH and Computational Center of the Moscow State University for the time on supercomputers *Chebyshev* and *Lomonosov*.

Note added in Proof: After this manuscript was accepted for publication, we have learned about the work of Haddon and coworkers [Sarkar, S.; Niyogi, S.; Bekyarova, E.; Haddon, R. C. *Chem. Sci.* **2011**, 2, 1326–1333] on the synthesis of the organometallic complexes of graphene and highly-oriented pyrolitic graphite with Cr|(C_6H_6) and Cr|($CO)_3$.

Supporting Information Available: Spin density, difference density, and spin–charge separation hole in Cr(C_6H_6)($CO)_3$; band structure of G|Cr|(C_6H_6) systems I–V and VIII; band structures of the G|Cr|($CO)_3$ systems VI and VII. This material is available free of charge *via* the Internet at http://pubs.acs.org.

REFERENCES AND NOTES

1. Novoselov, K. S.; Geim, A. K.; Morozov, S. V.; Jiang, D.; Zhang, Y.; Dubonos, S. V.; Grigorieva, I. V.; Firsov, A. A. Electric Field Effect in Atomically Thin Carbon Films. *Science* **2004**, *306*, 666–669.
2. Novoselov, K. S.; Geim, A. K.; Morozov, S. V.; Jiang, D.; Katsnelson, M. I.; Dubonos, S. V.; Grigorieva, I. V.; Firsov, A. A. Two-Dimensional Gas of Massless Dirac Fermions in Graphene. *Nature* **2005**, *438*, 197–200.
3. Novoselov, K. S.; McCann, E.; Morozov, S. V.; Falko, V. I.; Katsnelson, M. I.; Zeitler, U.; Jiang, D.; Schedin, F.; A. K. Geim, A. K. Unconventional Quantum Hall Effect and Berry's Phase of 2π in Bilayer Graphene. *Nat. Phys.* **2006**, *2*, 177–180.
4. Zhang, Y.; Tan, Y.; Stormer, H. L.; Kim, P. Experimental Observation of the Quantum Hall Effect and Berry's Phase in Graphene. *Nature* **2005**, *438*, 201–204.
5. Nomura, K.; MacDonald, A. H. Quantum Hall Ferromagnetism in Graphene. *Phys. Rev. Lett.* **2006**, *96*, 256602.
6. Nakada, K.; Fujita, M.; Dresselhaus, G.; Dresselhaus, M. S. Edge State in Graphene Ribbons: Nanometer Size Effect and Edge Shape Dependence. *Phys. Rev. B* **1996**, *54*, 17954–17961.
7. Son, Y.; Cohen, M. L.; Louie, S. G. Half-Metallic Graphene Nanoribbons. *Nature* **2006**, *444*, 347–349.
8. Hill, E.; Geim, A.; Novoselov, K.; Schedin, F.; Blake, P. Graphene Spin Valve Devices. *IEEE Trans. Magn.* **2006**, *42*, 2694–2696.
9. Brar, V. W.; Decker, R.; Solowan, H.-M.; Wang, Y.; Maserati, L.; Chan, K. T.; Lee, H.; Girit, C. O.; Zettl, A.; Louie, S. G.; Cohen, M. L.; Crommie, M. F. Gate-Controlled Ionization and Screening of Cobalt Adatoms on a Graphene Surface. *Nat. Phys.* **2011**, *7*, 43–47.
10. Kunstmann, J.; Ozdogbrevean, C.; Quandt, A.; Fehske, H. Stability of Edge States and Edge Magnetism in Graphene Nanoribbons. *Phys. Rev. B* **2011**, *83*, 045414.
11. Feynman, R. P. Quantum Mechanical Computers. *Opt. News* **1985**, *11*, 11–20.
12. Feynman, R. P. Quantum Mechanical Computers. *Found. Phys.* **1986**, *16*, 507–531.
13. Bloch, I. Ultracold Quantum Gases in Optical Lattices. *Nat. Phys.* **2005**, *1*, 23–30.
14. Jaksch, D.; Bruder, C.; Cirac, J. I.; Gardiner, C. W.; Zoller, P. Cold Bosonic Atoms in Optical Lattices. *Phys. Rev. Lett.* **1998**, *81*, 3108–3111.
15. Micheli, A.; Daley, A. J.; Jaksch, D.; Zoller, P. Single Atom Transistor in a 1D Optical Lattice. *Phys. Rev. Lett.* **2004**, *93*, 140408.
16. Morton, J.; Tyryshkin, A.; Ardavan, A.; Benjamin, S.; Porfyrakis, K.; Lyon, S.; Briggs, G. Bang-Bang Control of Fullerene Qubits Using Ultra-Fast Phase Gates. *Nat. Phys.* **2006**, *2*, 40–43.
17. Benjamin, S. C.; Benjamin, S. C.; Ardavan, A .; Briggs, G. A. D.; Britz, D. A.; Gunlycke, D.; Jefferson, J.; Jones, M. A. G.; Leigh, D. F.; Lovett, B. W.; *et al.* Towards a Fullerene-Based Quantum Computer. *J. Phys.: Condens. Matter* **2006**, *18*, 867–883.
18. Harneit, W. Fullerene-Based Electron-Spin Quantum Computer. *Phys. Rev. A* **2002**, *65*, 032322.
19. Warner, J. H.; Watt, A. A. R.; Ge, L.; Porfyrakis, K.; Akachi, T.; Okimoto, H.; Ito, Y.; Ardavar, A.; Montanari, B.; Jefferson, J. H.; *et al.* Dynamics of Paramagnetic Metallofullerenes in Carbon Nanotube Peapods. *Nano Lett.* **2008**, *8*, 1005–1010.
20. Elschenbroich, Ch. *Organometallics*; Wiley-VCH: Weinheim, 2006.

21. Kamegawa, T.; Sakai, T.; Matsuoka, M.; Anpo, M. Preparation and Characterization of Unique Inorganic-Organic Hybrid Mesoporous Materials Incorporating Arenetricarbonyl Complexes [-$C_6H_4M(CO)_3$-] (M = Cr, Mo). *J. Am. Chem. Soc.* **2005**, *127*, 16784–16785.
22. Vandersypen, L. M. K.; Steffen, M.; Breyta, G.; Yannoni, C. S.; Sherwood, M. H.; Chuang, I. L. *Nature* **2001**, *414*, 883–887.
23. Raebiger, H.; Lany, S.; Zunger, A. Charge Self-Regulation upon Changing the Oxidation State of Transition Metals in Insulators. *Nature* **2008**, *453*, 763–766.
24. Popov, A. A.; Dunsch, L. Hindered Cluster Rotation and ^{45}Sc Hyperfine Splitting Constant in Distonoid Anion Radical $Sc_3N@C_{80}^-$, and Spatial Spin-Charge Separation as a General Principle for Anions of Endohedral Fullerenes with Metal-Localized Lowest Unoccupied Molecular Orbitals. *J. Am. Chem. Soc.* **2008**, *130*, 17726–17742.
25. Lehtinen, P. O.; Foster, A. S.; Ayuela, A.; Krasheninnikov, A.; Nordlund, K.; Nieminen, R. M. Magnetic Properties and Diffusion of Adatoms on a Graphene Sheet. *Phys. Rev. Lett.* **2003**, *91*, 017202.
26. Sevincli, H.; Topsakal, M.; Durgun, E.; Ciraci, S. Electronic and Magnetic Properties of 3d Transition-Metal Atom Adsorbed Graphene and Graphene Nanoribbons. *Phys. Rev. B* **2008**, *77*, 195434.
27. Cao, C.; Wu, M.; Jiang, J.; Cheng, H.-P. Transition Metal Adatom and Dimer Adsorbed on Graphene: Induced Magnetization and Electronic Structures. *Phys. Rev. B* **2010**, *81*, 205424.
28. Liu, X.; Wang, C. Z.; Yao, Y. X.; Lu, W. C.; Hupalo, M.; Tringides, M. C.; Ho, K. M. Bonding and Charge Transfer by Metal Adatom Adsorption on Graphene. *Phys. Rev. B* **2011**, *83*, 235411.
29. Valencia, H.; Gil, A.; Frapper, G. Trends in the Adsorption of 3d Transition Metal Atoms onto Graphene and Nanotube Surfaces: A DFT Study and Molecular Orbital Analysis. *Phys. Chem. C* **2010**, *114*, 14141–14153.
30. Mao, Y.; Yuan, J.; Zhong, J. Density Functional Calculation of Transition Metal Adatom Adsorption on Graphene. *J. Phys.: Condens. Matter* **2008**, *20*, 115209.
31. Xiao, R.; Fritsch, D.; Kuz'min, M. D.; Koepernik, K.; Eschrig, H.; Richter, M.; Vietze, K.; Seifert, G. Co Dimers on Hexagonal Carbon Rings Proposed as Subnanometer Magnetic Storage Bits. *Phys. Rev. Lett.* **2009**, *103*, 187201.
32. Sargolzaei, M.; Gudarzi, F. Magnetic Properties of Single 3d Transition Metals Adsorbed on Graphene and Benzene: a Density Functional Theory Study. *J. Appl. Phys.* **2011**, *110*, 064303.
33. Johll, H.; Wu, J.; Ong, S. W.; Kang, H. C.; Tok, E. S. Graphene-adsorbed Fe, Co, and Ni Trimers and Tetramers: Structure, Stability, and Magnetic Moment. *Phys. Rev. B* **2011**, *83*, 205408.
34. Zolyomi, V.; Rusznyak, A.; Koltai, J.; Kurti, J.; Lambert, C. J. Functionalization of Graphene with Transition Metals. *Phys. Status Solidi B* **2010**, *247*, 2920–2923.
35. Hu, L.; Hu, X.; Wu, X.; Du, C.; Dai, Y.; Deng, J. Density Functional Calculation of Transition Metal Adatom Adsorption on Graphene. *J. Phys.: Condens. Matter* **2010**, *405*, 3337–3341.
36. Andrews, J. T. S.; Westrum, E. F.; Bjerrum, N. Heat Capacity and Vapor Pressure of Crystalline Bis(benzene)chromium. Third-Law Entropy Comparison and Thermodynamic Evidence Concerning the Structure of Bis(benzene) chromium. *J. Org. Chem.* **1969**, *17*, 293–302.
37. Wassmann, T.; Seitsonen, A. P.; Saitta, A. M.; Lazzeri, M.; Mauri, F. Clar's Theory, π-Electron Distribution, and Geometry of Graphene Nanoribbons. *J. Am. Chem. Soc.* **2010**, *132*, 3440–3451.
38. Hein, F. Zur Frage der Struktur der Chrom-phenyl-Verbindungen. Bemerkungen zur Abhandlung von E. O. Fischer und D. Seus. *Chem. Ber.* **1956**, *89*, 1816–1821.
39. Dedkov, Y. S.; Fonin, M.; Rudiger, U.; Laubschat, C. Rashba Effect in the Graphene/Ni(111) System. *Phys. Rev. Lett.* **2008**, *100*, 107602.
40. Guest, M. F.; Hillier, I. H.; Higginson, B. R.; Lloyd, D. R. The Electronic Structure of Transition Metal Complexes Containing Organic Ligands. II. Low-Energy Photoelectron-Spectra and *ab-initio* SCF-MO Calculations of Dibenzene Chromium and Benzene Chromium Tricarbonyl. *Mol. Phys.* **1975**, *29*, 113–128.
41. Prins, R.; Reinders, F. J. Electron Spin Resonance Measurements of Dibenzenechromium Cation. *Chem. Phys. Lett.* **1969**, *3*, 45–48.
42. Popov, A. A.; Chen, C.; Yang, S.; Lipps, F.; Dunsch, L. Spin-Flow Vibrational Spectroscopy of Molecules with Flexible Spin Density: Electrochemistry, ESR, Cluster and Spin Dynamics, and Bonding in $TiSc_2N@C_{80}$. *ACS Nano* **2010**, *4*, 4857–4871.
43. Silkin, V. M.; Zhao, J.; Guinea, F.; Chulkov, E. V.; Echenique, P. M.; Petek, H. Image Potential States in Graphene. *Phys. Rev. B* **2009**, *80*, 121408.
44. Kirwan, D. F.; Rocha, C. G.; Costa, A. T.; Ferreira, M. S. Sudden Decay of Indirect Exchange Coupling Between Magnetic Atoms on Carbon Nanotubes. *Phys. Rev. B* **2008**, *77*, 085432.
45. Bruno, P.; Chappert, C. Ruderman-Kittel Theory of Oscillatory Interlayer Exchange Coupling. *Phys. Rev. B* **1992**, *46*, 261–270.
46. Chen, J.-H.; Li, L.; Cullen, W. G.; Williams, E. D.; Fuhrer, M. S. Tunable Kondo Effect in Graphene with Defects. *Nat. Phys.* **2011**, *7*, 535–538.
47. Dirac, P. A. M. The Quantum Theory of the Electron. *Proc. R. Soc. A* **1928**, *117*, 610–624.
48. Won, H.; Maki, K. d-Wave Superconductor as a Model of High-T_c Superconductors. *Phys. Rev. B* **1994**, *49*, 1397–1402.
49. McGlinchey, M. J.; Wong, M. W. π-Complexed Polyfluoroarenes: a Reactivity, Bonding and Spectroscopic study of (η^6-C_6F_6)Cr(η^6-C_6H_6) and Related Molecules. *New J. Chem.* **2011**, *35*, 2066–2073.
50. Humphrey, W.; Dalke, A.; Schulte, K. VMD: Visual Molecular Dynamics. *J. Mol. Graphics* **1996**, *14*, 33–38.
51. Kresse, G.; Furthmuller, J. Efficient Iterative Schemes for *ab initio* Total-Energy Calculations Using a Plane-Wave Basis Set. *Phys. Rev. B* **1996**, *54*, 11169–11186.
52. Perdew, J. P.; Burke, K.; Ernzerhof, M. Generalized Gradient Approximation Made Simple. *Phys. Rev. Lett.* **1996**, *77*, 3865–38686.
53. Vanderbilt, D. Soft Self-Consistent Pseudopotentials in a Generalized Eigenvalue Formalism. *Phys. Rev. B* **1990**, *41*, 7892–7895.
54. Laikov, D. N. Fast Evaluation of Density Functional Exchange-Correlation Terms Using the Expansion of the Electron Density in Auxiliary Basis Sets. *Chem. Phys. Lett.* **1997**, *281*, 151–156.
55. Laikov, D. N. A New Class of Atomic Basis Functions for Accurate Electronic Structure Calculations of Molecules. *Chem. Phys. Lett.* **2005**, *416*, 116–120.
56. Neese, F. *ORCA*, An *ab initio*, Density Functional and Semiempirical Program Package, Version 2.7; Institute for Physical and Theoretical Chemistry: Bonn, 2009.
57. Becke, A. D. Density-Functional Exchange-Energy Approximation with Correct Asymptotic Behaviour. *Phys. Rev. A* **1998**, *38*, 3098–3100.
58. Lee, C.; Yang, W.; Parr, R. G. Development of the Colle-Salvetti Correlation-Energy Formula into a Functional of the Electron Density. *Phys. Rev. B* **1988**, *37*, 785–89.
59. Grimme, S. Semiempirical Hybrid Density Functional with Perturbative Second-Order Correlation. *J. Chem. Phys.* **2006**, *124*, 034108.
60. Neese, F.; Schwabe, T.; Grimme, S. Analytic Derivatives for Perturbatively Corrected "Double Hybrid" Density Functionals: Theory, Implementation and Applications. *J. Chem. Phys.* **2007**, *126*, 124115.
61. Grimme, S. Semiempirical GGA-Type Density Functional Constructed with a Long-Range Dispersion Correction. *J. Comput. Chem.* **2006**, *27*, 1787–1799.
62. Weigend, F.; Ahlrichs, R. Balanced Basis Sets of Split Valence, Triple Zeta Valence and Quadruple Zeta Valence Quality for H to Rn: Design and Assessment of Accuracy. *Phys. Chem. Chem. Phys.* **2005**, *7*, 3297–3305.
63. Zhao, Y.; Truhlar, D. G. A New Local Density Functional for Main-Group Thermochemistry, Transition Metal Bonding, Thermochemical Kinetics, and Noncovalent Interactions. *J. Chem. Phys.* **2006**, *125*, 194101.
64. Frisch, M. J.; Trucks, G. W.; Schlegel, H. B.; Scuseria, G. E.; Robb, M. A.; Cheeseman, J. R.; Scalmani, G.; Barone, V.;

Mennucci, B.; Petersson, A.; *et al*. *Gaussian 09*, revision A.02; Gaussian, Inc.: Wallingford, CT, 2009.
65. Firefly QC Package, which is Partially Based on the GAMESS (US) Source Code. Granovsky, A. A. *Firefly* version 7.1. G, http://classic.chem.msu.su/gran/firefly/index.html.
66. Schmidt, M. W.; Baldridge, K. K.; Boatz, J. A.; Elbert, S. T.; Gordon, M. S.; Jensen, J. H.; Koseki, S.; Matsunaga, N.; Nguyen, K. A.; Su, S.; *et al*. General Atomic and Molecular Electronic Structure System. *J. Comput. Chem.* **1993**, *14*, 1347–1363.
67. The CP2K developers group (2010), http://cp2k.berlios.de.
68. Lippert, G.; Hutter, J.; Parrinello, M. The Gaussian and Augmented-Plane-Wave Density Functional Method for *Ab Initio* Molecular Dynamics Simulation. *Theor. Chem. Acc.* **1993**, *103*, 124–140.
69. Goedecker, S.; Teter, M.; Hutter, J. Separable Dual-Space Gaussian Pseudopotentials. *J. Phys. Rev. B* **1996**, *54*, 1703–1710.
70. VandeVondele, J.; Krack, M.; Mohamed, F.; Parrinello, M.; Chassaing, T.; Hutter, J. Quickstep: Fast and Accurate Density Functional Calculations Using a Mixed Gaussian and Plane Waves Approach. *Comput. Phys. Commun.* **2005**, *167*, 103–128.